Investigation and Characterization of Cell Aggregation During and After Inkjet-Based Bioprinting of Cell-Laden Bioink

Heqi Xu
Department of Industrial, Manufacturing, and Systems Engineering,
Texas Tech University,
Lubbock, TX 79409
e-mail: heqi.xu@ttu.edu

Dulce Maria Martinez Salazar
Department of Mechanical Engineering,
Texas Tech University,
Lubbock, TX 79409
e-mail: dulmarti@ttu.edu

Md Shahriar
Department of Industrial, Manufacturing, and Systems Engineering,
Texas Tech University,
Lubbock, TX 79409
e-mail: md.shahriar@ttu.edu

Changxue Xu[1]
Department of Industrial, Manufacturing, and Systems Engineering,
Texas Tech University,
Lubbock, TX 79409
e-mail: changxue.xu@ttu.edu

Recently, 3D bioprinting techniques have been broadly recognized as a promising tool to fabricate functional tissues and organs. The bioink used for 3D bioprinting consists of biological materials and cells. Because of the dominant gravitational force, the suspended cells in the bioink sediment resulting in the accumulation and aggregation of cells. This study primarily focuses on the quantification of cell sedimentation-induced cell aggregation during and after inkjet-based bioprinting. The major conclusions are summarized as follows: (1) as the printing time increases from 0 min to 60 min, the percentage of the cells forming cell aggregates at the bottom of the bioink reservoir increases significantly from 3.6% to 54.5%, indicating a severe cell aggregation challenge in 3D bioprinting, (2) during inkjet-based bioprinting, at the printing time of only 15 min, more than 80% of the cells within the nozzle have formed cell aggregates. Both the individual cells and cell aggregates tend to migrate to the vicinity of the nozzle centerline mainly due to the weak shear-thinning properties of the bioink, and (3) after the bioprinting process, the mean cell number per microsphere increases significantly from 0.38 to 1.05 as printing time increases from 0 min to 15 min. The maximum number of cells encapsulated within one microsphere is ten, and 29.8% of the microspheres with cells encapsulated have contained small or large cell aggregates at the printing time of 15 min.
[DOI: 10.1115/1.4054640]

Keywords: inkjet-based bioprinting, cell sedimentation, cell aggregation, post-printing cell distribution, additive manufacturing, biomedical manufacturing

1 Introduction and Background

Benefiting from the technical innovations in cell biology and materials science, 3D bioprinting, originating from 3D printing technologies, has brought a revolution to tissue engineering [1,2]. Typically, 3D bioprinting techniques for depositing the bioink into the 3D desired structures [3] can be classified into inkjet-based bioprinting, microextrusion-based bioprinting, laser-assisted bioprinting, and stereolithography-based bioprinting [4]. Inkjet-based bioprinting, which accurately delivers small size and volume of cell-laden droplets at predefined locations onto a substrate relying on either thermal expansion or piezoelectric actuation, has been favored for various applications due to its unique non-contact delivery mechanism [5–7]. Bioink, as an essential element of 3D bioprinting, is usually composed of biological materials and living cells [8]. Holding the advantages of high water content and the similarity to natural extracellular matrix, hydrogels have been widely recognized as suitable biological materials for 3D bioprinting [9]. Briefly, the currently available hydrogels can be mainly divided into natural hydrogels (e.g., collagen [10] and fibrin [11]), synthetic hydrogels (e.g., poly(ethylene glycol) [12], poly(ethylene glycol) diacrylate [13], gelatin methacryloyl [14], and methacrylated hyaluronic acid [15]), and a mixture of natural and synthetic hydrogels [16]. As the other key component of the bioink, various types of living cells including but not limited to bone-marrow-derived human mesenchymal stem cells [17] and fibroblasts [18] have been incorporated into the fabrication of artificial tissues/organs such as liver [19] and heart [20].

The printing performance of 3D bioprinting is critical for the functionality of the 3D artificial tissues/organs. There are several factors affecting the printing performance through the uniformity of the living cells. Cell sedimentation and its induced cell aggregation are the two typical factors. For the bioink with a low viscosity, the fluid is always unable to provide enough buoyant force to counteract the gravitational force. Therefore, driven by the gravitational force, the suspended cells sediment resulting in the non-uniformity of the cell distribution within the bioink. Several studies have reported the significance of cell sedimentation on the printing performance. For example, Saunders et al. have reported an unstable printing process after 20 min printing due to the cell sedimentation [21]. Saunders and Derby reported an uneven number of cells per drop caused by the cell sedimentation [22]. Recently, there have been several studies focusing on the study of the sedimentation behaviors of cells. For instance, Wang and Belovich [23] presented a simple approach to measure the cell sedimentation velocity and derived a formula to analytically characterize the cell sedimentation velocity based on Stokes's law. Xu et al. [24] analyzed the force balance of a single cell in inkjet printing of the bioink containing 0.5–4% (w/v) sodium alginate and 5×10^5 fibroblasts/ml. The effects of the polymer concentration and printing time on the cell sedimentation velocity and the cell concentration were investigated systematically. It was reported that the cell sedimentation velocity was in the range of 0–1.5 μm/s, and the cell concentration at the bottom of the bioink reservoir could be four times higher after 2 h printing.

The cell sedimentation results in a significant increase in the local cell concentration at the bottom of the bioink. When the distance between adjacent cells becomes sufficiently small, the cells adhere to each other to form cell aggregates through cell-cell interaction. Parsa et al. observed cell aggregates with a size of more than 200 μm after 10 min printing time [25]. Meanwhile, severe cell aggregation was still observed within a 3 h printing period although continuous stirring was applied to the bioink reservoir. In addition, it has been well documented that the cell aggregation negatively affected the printing performance [26]. For example, Zhang et al. reported that the cell aggregation due to the interaction of living cells changed the rheological properties such as the viscosity of

[1]Corresponding author.
Manuscript received March 24, 2022; final manuscript received May 18, 2022; published online June 22, 2022. Assoc. Editor: Robert Chang.

the bioink, which resulted in non-ideal jetting behaviors and non-uniformity of cell distribution during laser-assisted bioprinting [27]. In addition, when the size of the cell aggregate became comparable to the nozzle orifice size, nozzle clogging occurred and jetting was discontinued [28]. In summary, the cell aggregation due to the cell sedimentation significantly affects the printing reliability and performance in terms of the jetting behaviors, the non-uniformity of cell distribution, and even nozzle clogging [29].

The earlier studies have focused on the quantification of the cell sedimentation behaviors (e.g., cell sedimentation velocity and local cell concentration change due to the cell sedimentation) and brief observation of the cell aggregation phenomena. Even though the cell aggregation phenomenon has been broadly reported as a significant challenge in the existing literature, none of the studies have specifically focused on the investigation of the cell aggregation mechanism and the characterization of cell aggregation both during and after inkjet-based bioprinting. This is the first study focusing on the investigation and characterization of the cell aggregation during and after the printing process. Specifically, during the printing process, the cell aggregation is quantified within the bioink reservoir and inside the nozzle, and after the printing process, the cell aggregation is quantified within the formed microspheres. The following sections of this paper are listed as follows: Sec. 2 clearly lists the experimental conditions for this study and presents the characterization of the cell aggregation, Sec. 3 presents the detailed results of the cell aggregation during and after the printing process, and Sec. 4 draws the major conclusions for this study and proposes the future research directions.

2 Materials and Methods

2.1 Experimental Setup. The illustration of the inkjet-based bioprinting system used in this study is shown in Fig. 1. Briefly, there are several major components including an inkjet nozzle controlled by a piezo actuator, a bioink reservoir providing the bioink to the inkjet nozzle, a waveform generator, a high-resolution horizontal imaging system, a pneumatic controller, and a substrate receiving the cell-laden droplets. Specifically, in this study, sodium alginate with high water content and excellent biocompatibility was selected to provide the microenvironment for cell attachment, proliferation, and differentiation [30]. The 3T3 fibroblasts were selected to be suspended within 0.5% (w/v) sodium alginate solution with a cell concentration of 1.5×10^6 cells/ml. For more details regarding the experimental setup and materials refer to our earlier studies [18,31]. In this study, during the printing process, the cell aggregation is quantified within the bioink reservoir and inside the nozzle, and after the printing process, the cell aggregation is quantified within the formed microspheres.

2.2 Cell Aggregation Characterization. The cell aggregates are classified into three types: individual cells without aggregation, small aggregates with 2–4 cells, and large aggregates with at least five cells. The percentage of individual cells without aggregation was characterized using the following equation

$$ic\% = \frac{\sum_{a=1}^{1} ab}{\sum_{a=1}^{c} ab} \times 100\% \tag{1}$$

where $ic\%$ represents the percentage of individual cells without aggregation, a represents the number of the cells in the individual cells or cell aggregates, b represents the associated counting frequency of individual cells or cell aggregates, and c represents the largest cell aggregate with the maximum number of individual cells. The percentage of the cells forming small aggregates was characterized using the following equation:

$$sa\% = \frac{\sum_{a=2}^{4} ab}{\sum_{a=1}^{c} ab} \times 100\% \tag{2}$$

where $sa\%$ represents the percentage of the cells forming small cell aggregates. The percentage of the cells forming large aggregates was characterized using the following equation:

$$la\% = \frac{\sum_{a=5}^{c} ab}{\sum_{a=1}^{c} ab} \times 100\% \tag{3}$$

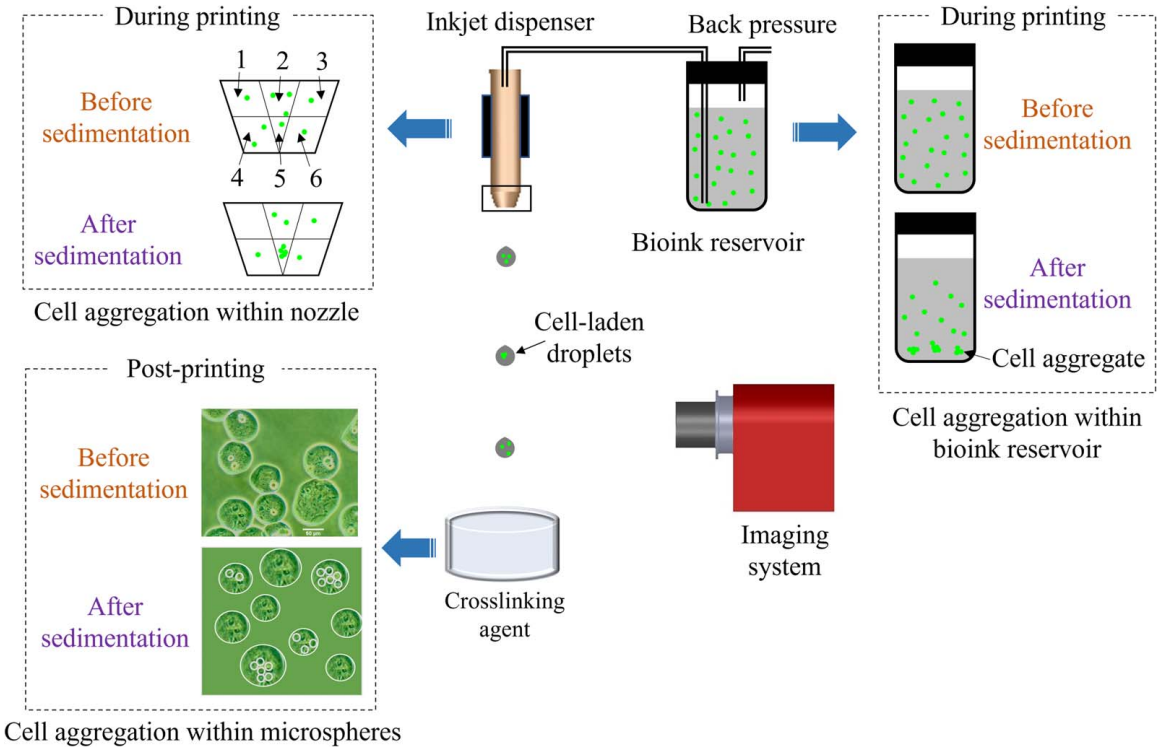

Fig. 1 Schematic diagram of the experimental setup. Cell aggregation is characterized during and after the printing process.

where *la%* is the percentage of the cells forming large cell aggregates.

During the printing process, the cell aggregation is quantified within the bioink reservoir and inside the nozzle. Within the bioink reservoir, a small amount of bioink was collected and observed using a hemocytometer at a printing time of 0–60 min with an interval of 20 min. Experiments were repeated three times at each condition. Within the transparent inkjet nozzle (MicroFab Technologies, Plano, TX), a time-resolved imaging system (ImageXpert, Nashua, NH) was utilized to capture the images and characterize cell aggregation and spatial distribution within the nozzle at the printing time of 0 min and 15 min. The reason for selecting different printing times for the characterization of cell aggregation within the bioink reservoir and inkjet nozzle is the different severity of cell aggregation. Cell aggregation is more severe within the inkjet nozzle. With a longer printing time, larger sizes of the three-dimensional cell aggregates are formed within the nozzle which increase the difficulty of accurately differentiating and counting the number of individual cells composing the cell aggregates. The nozzle was divided into six regions and marked as 1–6 shown in Fig. 1. At each condition, 100 images were captured to measure the cell aggregation percentage in each region. Inside the nozzle, the bioink flow is driven by the complex pressure wave. The suspended individual cells or cell aggregates are affected by the flow and may migrate in different directions. Hence, the nozzle inside space was divided into six regions. Regions 1 and 3 are on the top close to the nozzle inner wall, regions 4 and 6 are at the bottom close to the nozzle inner wall, and regions 2 and 5 are in the vicinity of the nozzle centerline on the top and at the bottom, respectively. In addition, after the printing process, the cell aggregation is quantified within the formed microspheres at the printing time of 0 min and 15 min. A thousand microspheres were randomly selected to quantify the mean cell number within the microspheres, and the percentages of microspheres containing individual cells, small aggregates, and large aggregates were characterized, respectively [32]. For the cell aggregation within the bioink reservoir, a one-way analysis of variance was performed to check the significance of printing time on cell aggregation where $P < 0.05$ indicated a statistically significant effect. For the cell aggregation within the inkjet nozzle and microspheres, a *t*-test was performed to check the significance of printing time on cell aggregation where $P < 0.05$ indicated a statistically significant effect.

3 Results and Discussions

Using the bioink with a low polymer concentration in inkjet-based bioprinting, the cells are driven by the dominant gravitational force to sediment resulting in the accumulation of cells at the bottom of the bioink reservoir. Therefore, the cell-cell distance is reduced resulting in the enhancement of cell-cell interaction force and facilitation of cell aggregation [33]. Specifically, Sec. 3.1 investigates the cell aggregation at the bottom of the bioink reservoir during the bioprinting process. The percentage of the cells forming individual cells and cell aggregates are characterized after 0 min, 20 min, 40 min, and 60 min printing time, respectively. Section 3.2 focuses on the formation and distribution of individual cells and cell aggregates within the inkjet nozzle during the bioprinting process. Section 3.3 investigates the distribution of individual cells and cell aggregates within the formed microspheres after the bioprinting process.

3.1 Investigation of Cell Aggregation Within the Bioink Reservoir During Printing. At the beginning of the printing process, the cells in the bioink are suspended uniformly within the bioink reservoir. With the increase of the printing time, the cells sediment to the bottom of the bioink reservoir, resulting in the cell aggregation. Figure 2 representatively shows the effect of the printing time on the cell aggregation at the bottom of the bioink reservoir. It is seen that with the increase of the printing time, the percentage of the individual cells decreases significantly while the percentage of the cells forming small and large aggregates increases significantly. As the printing time increases from 0 min to 20 min to 40 min to 60 min, the percentage of the individual cells decreases significantly from 96.4% to 77% to 70% to 45.5%, and the percentage of the cells forming small aggregates increases significantly from 3.6% to 23% to 30% to 42.7%. Large cell aggregates are only observed at 60 min printing time with an 11.8% percentage of the cells forming large aggregates. At the printing time of 0 min, 96.4% cells are individual cells without aggregation. However, at the printing time of 60 min, only 45.5% cells are individual cells, and small aggregates are 42.7%, and large aggregates are 11.8%. This indicates a severe cell aggregation phenomenon within the bioink reservoir during the bioprinting process. The *P*-value is less than 0.05 indicating the printing time has a significant effect on the cell aggregation.

3.2 Investigation of Cell Aggregation and Distribution Within the Inkjet Nozzle During Printing. During the bioprinting process, the bioink at the bottom of the bioink reservoir is transferred to the inkjet nozzle for the droplet formation process. The cell aggregation inside the nozzle is compared at the printing time of 0 min and 15 min as shown in Fig. 3. It is seen that at 0 min printing time, most of the cells within the inkjet nozzle are individual cells without aggregation. There are only 3.5% of the cells forming small cell aggregates, and no large cell aggregates are observed. However, at the printing time of 15 min, the percentage of the individual cells without aggregation dramatically decreases to 17.3%. There are 54.5% of the cells forming small cell aggregates composed of 2–4 cells, and 28.2% of the cells forming large cell aggregates composed of at least five cells. At the printing time of 0 min, only 3.5% cells form cell aggregates, while 82.7% cells form either small or large cell aggregates after 15 min indicating severe cell sedimentation and cell aggregation inside the nozzle during the printing process. The *P*-value is less than 0.05 indicating the printing time has a significant effect on the cell aggregation.

Inside the nozzle, the bioink flow is driven by the complex pressure wave. The suspended cells or cell aggregates are affected by the flow and may migrate in different directions. Hence, the nozzle inside space was divided into six regions. This is the first study investigating the spatial distributions of the cell aggregates in different regions within the nozzle shown in Fig. 4. At the printing time of 0 min, 96.5% cells are individual cells without aggregation. 55% of the individual cells are located in regions 2 and 5 shown in Fig. 4(*a*) indicating the cells tend to migrate to the vicinity of the nozzle centerline instead of the regions near the nozzle wall. At the printing time of 15 min, 17.3% cells are individual cells without aggregation. 64.4% of the individual cells shown in Fig. 4(*b*) are located in regions 2 and 5 which are the center regions of the nozzle inside space. In addition, in Fig. 4(*b*), 70.7% of the small aggregates and 99% of the large aggregates appear in regions 2 and 5. The observation of the cell aggregate distribution is similar to that of the individual cells. Compared to the individual cells, the cell aggregates seem to even more prefer the vicinity of the nozzle centerline. Almost all large cell aggregates are observed in the center region of the nozzle inside space. During the printing process, the bioink inside the nozzle is mainly subject to a shear flow driven by the complex pressure wave. The motion of the cells suspended in the bioink is significantly affected by the shear flow and bioink rheological properties [34]. The bioink has typical non-Newtonian shear-thinning properties. The measure of the viscosity under different shear rates is shown in Fig. 4(*a*) indicating weak shear-thinning properties. When the cells are subject to a shear flow at the weak shear-thinning effect of the bioink, the suspended cells tend to migrate towards the centerline of the nozzle where the shear is smaller [35]. In addition, the lift force induced by the wall also drives the particles to be away from the wall [36].

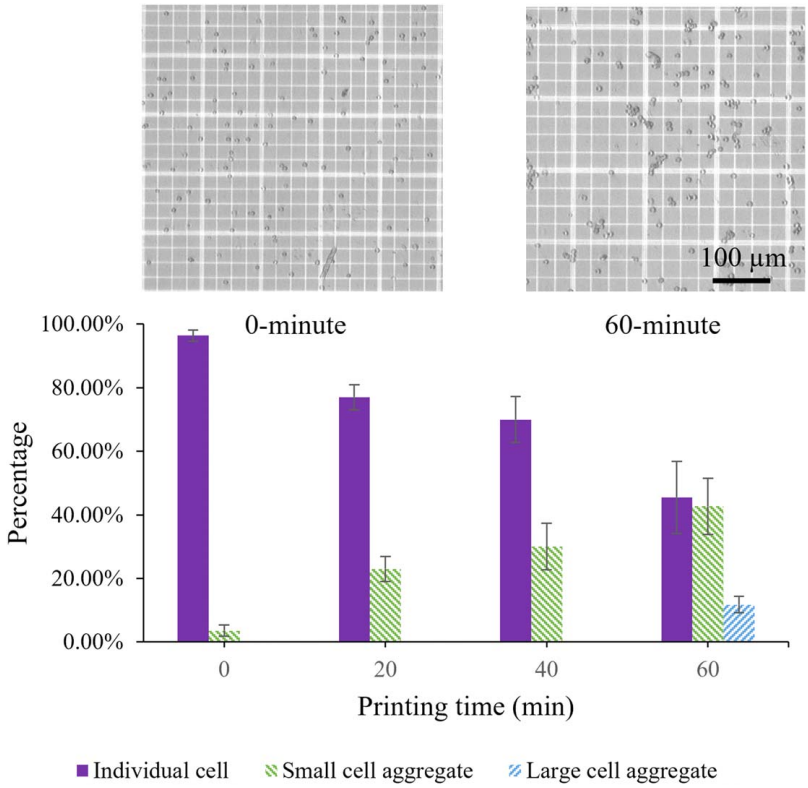

Fig. 2 Effect of the printing time on the cell aggregation at the bottom of the bioink reservoir. The inserted images representatively show the individual cells and cell aggregates at 0 min and 60 min printing time.

3.3 Investigation of Cell Aggregation and Distribution Within the Formed Microspheres After Printing. Initially, with a low cell concentration, most of the formed microspheres only contain zero or a few cells inside. And there are a few microspheres containing cell aggregates inside. However, as the cell concentration of the bioink is increased and the cell aggregation is facilitated due to the cell sedimentation, the number of the cells encapsulated within one microsphere generally increases, and the probability of one microsphere containing cell aggregates significantly increases. In this section, 1000 microspheres are selected to quantify the post-printing cell distribution demonstrating the distribution of cells within the formed microspheres. And the number

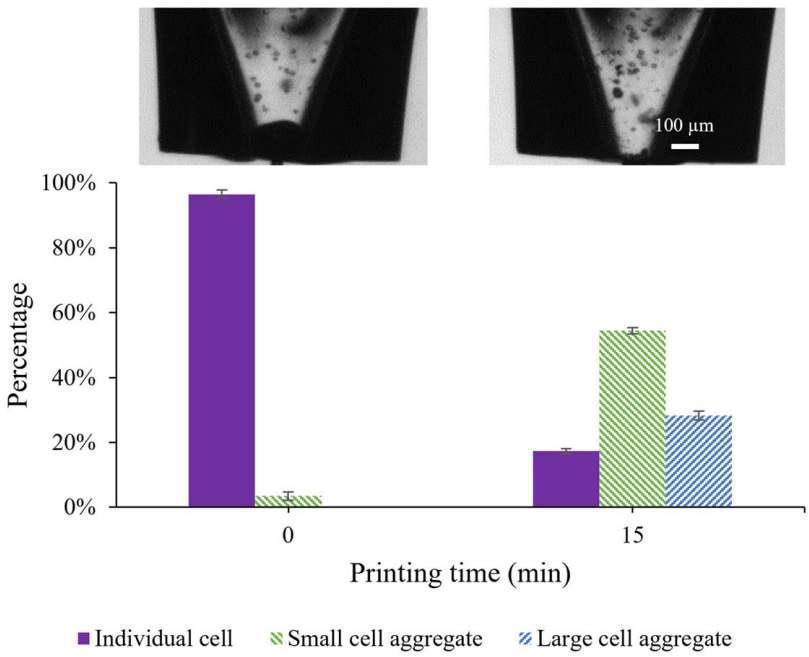

Fig. 3 Comparison of individual cells and cell aggregates within the inkjet nozzle at 0 min and 15 min printing time. The inserted images are representative images of the cells within the inkjet nozzle at different printing times.

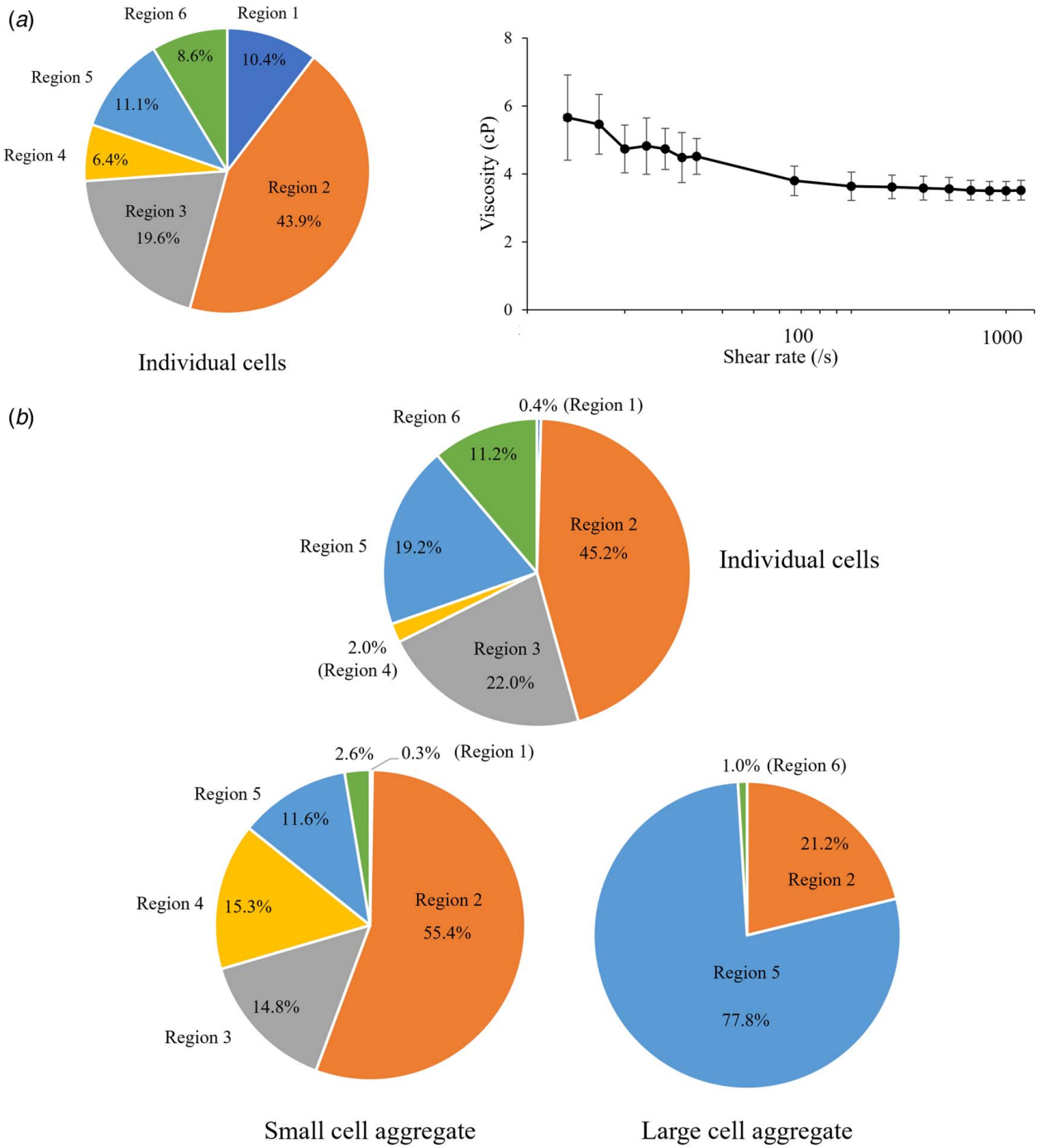

Fig. 4 (*a*) Cell spatial distribution within the inkjet nozzle at 0 min printing time, and bioink viscosity measurement showing weak shear-thinning properties and (*b*) spatial distribution of individual cells, small cell aggregates, and large cell aggregates within the inkjet nozzle at 15 min printing time

of microspheres only containing individual cells and small and large sizes of cell aggregates at different printing times is characterized and shown in Fig. 5.

The cell-laden droplets are deposited onto the substrate containing the crosslinking agent (2% (w/v) calcium chloride in this study). The cell-laden droplets are crosslinked to form microspheres with the living cells encapsulated. In this section, 1000 microspheres are randomly selected to quantify the post-printing cell distribution within the formed microspheres. Figure 5 shows the post-printing percentages of microspheres containing individual cells, small cell aggregates, and large cell aggregates at different printing times. At 0 min printing time, the maximum number of cells encapsulated within one microsphere is three. There are 68.7%, 25.5%, 4.1%, and 1.4% of the microspheres containing no cells, one single cell, two cells, and three cells, respectively. Among the microspheres with cell encapsulation, 95.5% microspheres contain individual cells without cell aggregation, 4.5% microspheres contain small aggregates with 2–4 cells, and 0% microspheres contain large aggregates with at least five cells. The mean cell number per microsphere is 0.38. At 15 min printing time, the maximum number of cells encapsulated within one microsphere is ten. There are 48.4%, 27.7%, 19.2%, and 4.7% of the microspheres containing no cells, one single cell, two to four cells, and at least five cells, respectively. Among the microspheres with cell encapsulation, 70.2%

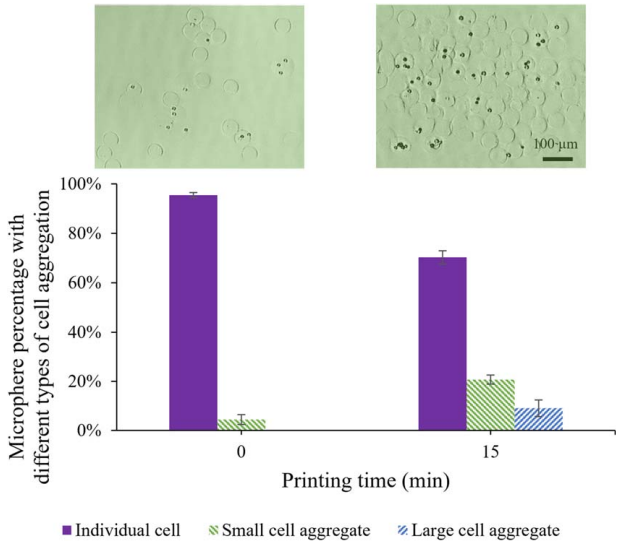

Fig. 5 Post-printing percentages of microspheres containing individual cells, small cell aggregates, and large cell aggregates at different printing times. The inserted images representatively show the post-printing cell distribution at different printing times.

microspheres contain individual cells without cell aggregation, 20.7% microspheres contain small aggregates with 2–4 cells, and 9.1% microspheres contain large aggregates with at least five cells. The mean cell number per microsphere is 1.05 indicating the increase in the local cell concentration due to the cell sedimentation. The *P*-value is less than 0.05 indicating the printing time has a significant effect on the cell aggregation.

4 Conclusions and Future Prospective

Recently, 3D bioprinting techniques have been broadly recognized as a promising tool to fabricate functional tissues and organs. The bioink used for 3D bioprinting consists of biological materials and cells. Because of the dominant gravitational force, the suspended cells in the bioink sediment result in the significant increase in the local cell concentration, which facilitates the cell aggregation. As reported in a recent study [37], higher viscosity of sodium alginate could help to mitigate cell sedimentation and aggregation. However, it is not wise to mitigate the cell sedimentation and aggregation simply by increasing the viscosity of the polymer solution since high-viscosity sodium alginate solution may easily cause nozzle clogging and reduce the printing performance. Cell aggregation is widely recognized as a critical challenge in 3D bioprinting, significantly affecting the printing reliability and quality. This paper is the first study focusing on the investigation of cell sedimentation-induced cell aggregation during and after inkjet-based bioprinting. The major conclusions are summarized as follows: (1) as the printing time increases from 0 min to 60 min, the percentage of the cells forming cell aggregates at the bottom of the bioink reservoir increases significantly from 3.6% to 54.5%, indicating a severe cell aggregation challenge in 3D bioprinting, (2) during inkjet-based bioprinting, at the printing time of only 15 min, more than 80% of the cells within the nozzle have formed cell aggregates. Both the individual cells and cell aggregates tend to migrate to the vicinity of the nozzle centerline mainly due to the weak shear-thinning properties of the bioink, and (3) after the bioprinting process, the mean cell number per microsphere increases significantly from 0.38 to 1.05 as printing time increases from 0 min to 15 min. The maximum number of cells encapsulated within one microsphere is ten, and 29.8% of the microspheres with cells encapsulated have contained small or large cell aggregates at the printing time of 15 min.

Future work may include a more comprehensive study on the cell aggregation and its effect on the printing performance during inkjet-based bioprinting of cell-laden bioink, and the development of an effective method to mitigate cell sedimentation and aggregation.

Acknowledgment

This work was partially supported by the National Science Foundation (NSF) (Grant No. CMMI-1762282).

Conflict of Interest

There are no conflicts of interest.

Data Availability Statement

The authors attest that all data for this study are included in the paper.

Nomenclature

- a = the number of the cells in the individual cells or cell aggregates
- b = the associated counting frequency of individual cells or cell aggregates
- c = the largest cell aggregate with the maximum number of individual cells
- $ic\%$ = the percentage of individual cells without aggregation
- $la\%$ = the percentage of the cells forming large cell aggregates
- $sa\%$ = the percentage of the cells forming small cell aggregates

References

[1] Zhang, B., Luo, Y., Ma, L., Gao, L., Li, Y., Xue, Q., Yang, H., and Cui, Z., 2018, "3D Bioprinting: An Emerging Technology Full of Opportunities and Challenges," Bio-Des. Manuf., **1**(1), pp. 2–13.

[2] Chen, R., Chang, R. C., Tai, B., Huang, Y., Ozdoganlar, B., Li, W., and Shih, A., 2020, "Biomedical Manufacturing: A Review of the Emerging Research and Applications," ASME J. Manuf. Sci. Eng., **142**(11), p. 110807.

[3] Thakare, K., Jerpseth, L., Qin, H., and Pei, Z., 2021, "Bioprinting Using Algae: Effects of Extrusion Pressure and Needle Diameter on Cell Quantity in Printed Samples," ASME J. Manuf. Sci. Eng., **143**(1), p. 014501.

[4] Li, J., Chen, M., Fan, X., and Zhou, H., 2016, "Recent Advances in Bioprinting Techniques: Approaches, Applications, and Future Prospects," J. Transl. Med., **14**(1), p. 271.

[5] Gudapati, H., Dey, M., and Ozbolat, I., 2016, "A Comprehensive Review on Droplet-Based Bioprinting: Past, Present and Future," Biomaterials, **102**, pp. 20–42.

[6] Li, X., Liu, B., Pei, B., Chen, J., Zhou, D., Peng, J., Zhang, X., Jia, W., and Xu, T., 2020, "Inkjet Bioprinting of Biomaterials," Chem. Rev., **120**(19), pp. 10793–10833.

[7] Nakamura, M., Kobayashi, A., Takagi, F., Watanabe, A., Hiruma, Y., Ohuchi, K., Iwasaki, Y., Horie, M., Morita, I., and Takatani, S., 2005, "Biocompatible Inkjet Printing Technique for Designed Seeding of Individual Living Cells," Tissue Eng., **11**(11–12), pp. 1658–1666.

[8] Gungor-Ozkerim, P. S., Inci, I., Zhang, Y. S., Khademhosseini, A., and Dokmeci, M. R., 2018, "Bioinks for 3D Bioprinting: An Overview," Biomater. Sci., **6**(5), pp. 915–946.

[9] Wang, S., Lee, J. M., and Yeong, W. Y., 2015, "Smart Hydrogels for 3D Bioprinting," Int. J. Bioprinting, **1**(1), pp. 3–14.

[10] Lee, A., Hudson, A., Shiwarski, D., Tashman, J., Hinton, T., Yerneni, S., Bliley, J., Campbell, P., and Feinberg, A., 2019, "3D Bioprinting of Collagen to Rebuild Components of the Human Heart," Science, **365**(6452), pp. 482–487.

[11] De Melo, B. A., Jodat, Y. A., Cruz, E. M., Benincasa, J. C., Shin, S. R., and Porcionatto, M. A., 2020, "Strategies to Use Fibrinogen as Bioink for 3D Bioprinting Fibrin-Based Soft and Hard Tissues," Acta Biomater., **117**, pp. 60–76.

[12] Parak, A., Pradeep, P., du Toit, L. C., Kumar, P., Choonara, Y. E., and Pillay, V., 2019, "Functionalizing Bioinks for 3D Bioprinting Applications," Drug Discov. Today, **24**(1), pp. 198–205.

[13] Jin, Y., Xiong, R., Antonelli, P. J., Long, C. J., McAleer, C. W., Hickman, J. J., and Huang, Y., 2021, "Nanoclay Suspension-Enabled Extrusion Bioprinting of Three-Dimensional Soft Structures," ASME J. Manuf. Sci. Eng., **143**(12), p. 121004.

[14] Thakare, K., Jerpseth, L., Pei, Z., and Qin, H., 2022, "Applying Layer-by-Layer Photo-Crosslinking in Green Bioprinting: Shape Fidelity and Cell Viability of

Printed Hydrogel Constructs Containing Algae Cells," ASME J. Manuf. Sci. Eng., **144**(9), p. 094502.
[15] Kesti, M., Müller, M., Becher, J., Schnabelrauch, M., D'Este, M., Eglin, D., and Zenobi-Wong, M., 2015, "A Versatile Bioink for Three-Dimensional Printing of Cellular Scaffolds Based on Thermally and Photo-Triggered Tandem Gelation," Acta Biomater., **11**, pp. 162–172.
[16] Patenaude, M., and Hoare, T., 2012, "Injectable, Mixed Natural-Synthetic Polymer Hydrogels With Modular Properties," Biomacromolecules, **13**(2), pp. 369–378.
[17] Gao, G., Schilling, A. F., Yonezawa, T., Wang, J., Dai, G., and Cui, X., 2014, "Bioactive Nanoparticles Stimulate Bone Tissue Formation in Bioprinted Three-Dimensional Scaffold and Human Mesenchymal Stem Cells," Biotechnol. J., **9**(10), pp. 1304–1311.
[18] Xu, C., Chai, W., Huang, Y., and Markwald, R. R., 2012, "Scaffold-Free Inkjet Printing of Three-Dimensional Zigzag Cellular Tubes," Biotechnol. Bioeng., **109**(12), pp. 3152–3160.
[19] Faulkner-Jones, A., Fyfe, C., Cornelissen, D.-J., Gardner, J., King, J., Courtney, A., and Shu, W., 2015, "Bioprinting of Human Pluripotent Stem Cells and Their Directed Differentiation Into Hepatocyte-Like Cells for the Generation of Mini-Livers in 3D," Biofabrication, **7**(4), p. 044102.
[20] Hockaday, L., Kang, K., Colangelo, N., Cheung, P., Duan, B., Malone, E., Wu, J., Girardi, L., Bonassar, L., and Lipson, H., 2012, "Rapid 3D Printing of Anatomically Accurate and Mechanically Heterogeneous Aortic Valve Hydrogel Scaffolds," Biofabrication, **4**(3), p. 035005.
[21] Saunders, R. E., Gough, J. E., and Derby, B., 2008, "Delivery of Human Fibroblast Cells by Piezoelectric Drop-On-Demand Inkjet Printing," Biomaterials, **29**(2), pp. 193–203.
[22] Saunders, R. E., and Derby, B., 2014, "Inkjet Printing Biomaterials for Tissue Engineering: Bioprinting," Int. Mater. Rev., **59**(8), pp. 430–448.
[23] Wang, Z., and Belovich, J. M., 2010, "A Simple Apparatus for Measuring Cell Settling Velocity," Biotechnol. Prog., **26**(5), pp. 1361–1366.
[24] Xu, H., Zhang, Z., and Xu, C., 2019, "Sedimentation Study of Bioink Containing Living Cells," J. Appl. Phys., **125**(11), p. 114901.
[25] Parsa, S., Gupta, M., Loizeau, F., and Cheung, K. C., 2010, "Effects of Surfactant and Gentle Agitation on Inkjet Dispensing of Living Cells," Biofabrication, **2**(2), p. 025003.
[26] Chahal, D., Ahmadi, A., and Cheung, K. C., 2012, "Improving Piezoelectric Cell Printing Accuracy and Reliability Through Neutral Buoyancy of Suspensions," Biotechnol. Bioeng., **109**(11), pp. 2932–2940.
[27] Zhang, Z., Xu, C., Xiong, R., Chrisey, D. B., and Huang, Y., 2017, "Effects of Living Cells on the Bioink Printability During Laser Printing," Biomicrofluidics, **11**(3), p. 034120.
[28] Lee, A., Sudau, K., Ahn, K. H., Lee, S. J., and Willenbacher, N., 2012, "Optimization of Experimental Parameters to Suppress Nozzle Clogging in Inkjet Printing," Ind. Eng. Chem. Res., **51**(40), pp. 13195–13204.
[29] Ringeisen, B. R., Othon, C. M., Barron, J. A., Young, D., and Spargo, B. J., 2006, "Jet-Based Methods to Print Living Cells," Biotechnol. J., **1**(9), pp. 930–948.
[30] Wu, D., and Xu, C., 2018, "Predictive Modeling of Droplet Formation Processes in Inkjet-Based Bioprinting," ASME J. Manuf. Sci. Eng., **140**(10), p. 101007.
[31] Xu, C., Zhang, M., Huang, Y., Ogale, A., Fu, J., and Markwald, R. R., 2014, "Study of Droplet Formation Process During Drop-On-Demand Inkjetting of Living Cell-Laden Bioink," Langmuir, **30**(30), pp. 9130–9138.
[32] Xu, H., Casillas, J., and Xu, C., 2019, "Effects of Printing Conditions on Cell Distribution Within Microspheres During Inkjet-Based Bioprinting," AIP Adv., **9**(9), p. 095055.
[33] Xu, H., Liu, J., Zhang, Z., and Xu, C., 2022, "Cell Sedimentation During 3D Bioprinting: A Mini Review," Bio-Des. Manuf., pp. 1–10.
[34] Cheng, E., Yu, H., Ahmadi, A., and Cheung, K. C., 2016, "Investigation of the Hydrodynamic Response of Cells in Drop on Demand Piezoelectric Inkjet Nozzles," Biofabrication, **8**(1), p. 015008.
[35] Zhou, J., and Papautsky, I., 2020, "Viscoelastic Microfluidics: Progress and Challenges," Microsyst. Nanoeng., **6**(1), p. 113.
[36] Yang, S., Lee, S. S., Ahn, S. W., Kang, K., Shim, W., Lee, G., Hyun, K., and Kim, J. M., 2012, "Deformability-Selective Particle Entrainment and Separation in a Rectangular Microchannel Using Medium Viscoelasticity," Soft Matter, **8**(18), pp. 5011–5019.
[37] Xu, H., Martinez Salazar, D. M., and Xu, C., 2022, "Investigation of Cell Concentration Change and Cell Aggregation Due to Cell Sedimentation During Inkjet-Based Bioprinting of Cell-Laden Bioink," Machines, **10**(5), p. 315.